# Effects of Abdominal Wall Morphology on Ultrasonic Pulse Distortion

Laura M. Hinkelman[1], T. Douglas Mast[2], Michael J. Orr[1], and Robert C. Waag[13]

[1]Dept. of Electrical Engineering, University of Rochester, Rochester, NY 14627
[2]Applied Research Laboratory, The Pennsylvania State University, University Park, PA 16802
[3]Dept. of Radiology, University of Rochester, Rochester, NY 14642

*Abstract*—**Wavefront propagation through the abdominal wall was investigated by measurements employing full-thickness specimens and their individual fat and muscle layers. These measurements confirm that both fat and muscle produce significant wavefront distortion and focus degradation. However, the spatial characteristics of the distortion produced by fat and muscle differ, and the total distortion produced by the abdominal wall is not the arithmetic sum of that produced by the individual layers. The interface between the muscle and subcutaneous fat layers, which consists of a thin layer of connective tissue, was found to be smooth or slightly curved. Distortion produced by different tissues was further characterized by simulations using a finite-difference time-domain implementation of the linearized wave propagation equations for a lossless inhomogeneous fluid. Scanned images of six human abdominal wall cross sections provided the data for the propagation media in the simulation. The images were mapped into regions of fat, muscle, and connective tissue, each of which was assigned a uniform sound speed and density obtained from literature values. The computed wavefronts contained arrival time, energy level, and wave shape distortion similar to that in measurements. Visualization of wave propagation within the tissue cross sections suggests that most arrival time distortion is produced by acoustic path length differences while amplitude and waveform variations are the result of scattering from inhomogeneities. Many arrival time fluctuation and energy level fluctuation features could be traced to specific anatomical structures. These results indicate that wavefront distortion, apart from bulk attenuation effects, is primarily caused by tissue structures and inhomogeneities rather than refraction at layer interfaces.**

## I. Introduction

Wavefront distortion is considered to be a significant obstacle to improved ultrasonic image quality. Direct measurements [1],[2] have yielded parameters describing wavefront distortion produced by the abdominal wall, but have provided little insight into the source of the distortion. Greater knowledge of the mechanisms that cause wavefront distortion would improve understanding of what is required for success in adaptive abdominal ultrasonic imaging.

A few investigators have attempted to improve understanding of wavefront distortion through the use of simulations. However, most of these simulations have been based on simple assumptions about the structure of the body wall and the causes of wavefront distortion. For example, in Ref. [3], ray-tracing techniques limited to refraction effects and simple tissue geometries were used. Berkhoff *et al.*[4] used a more complete computational technique (the conjugate gradient Rayleigh method), but considered only the effect of propagation through an irregular interface.

Recently, a simulation technique that includes all wave effects was applied to tissue models based on images of actual human abdominal wall cross sections [5]. This finite-difference time-domain simulation produced arrival time, energy level, and wave shape distortion similar to that measured for the same abdominal wall specimens.

The study described here employs this simulation technique and new measurements to examine the causes of ultrasonic wavefront distortion in the abdominal wall. In particular, the relative contributions of the fat and muscle layers to distortion and the importance of the interface between these layers are investigated.

## II. Method

### A. Measurements

Six fresh unfixed abdominal wall specimens were obtained from autopsy and stored at −20°C. Each specimen was later thawed and reference lines for positioning were ruled on its skin surface. The specimen was then pressurized to 500 p.s.i. for 30 min. to eliminate air bubbles within the tissue. The wavefront distortion produced by the whole specimen was then measured according to the procedure detailed in Ref. [2]. The specimen was suspended between 7.5 $\mu$m thick polyimide membranes in a 37.0°C water bath. Since the membranes held the specimens so that their smooth outer surfaces (the skin and peritoneum) were approximately parallel, refraction or scattering from water-tissue boundaries did not contribute significantly to the measured distortion. Ultrasonic pulses at a nominal center frequency of 3.75 MHz were emitted from a hemispheric source placed about 165 mm below the specimen. Data were recorded on each of the 128 elements of a 0.72 mm pitch, 3.75 MHz linear array positioned 5-10 mm above the specimen's skin surface. A foam mask reduced the active elevation of the array to 1.44 mm. The array was translated 32 times in the elevation direction to synthesize a $92.16 \times 46.08\ \mathrm{mm}^2$ aperture. The position of each measurement relative to the markings on the specimen was noted.

After the distortion measurement, the specimen was divided at the septum between the subcutaneous fat and the

Funding for this investigation was provided by the University of Rochester Diagnostic Ultrasound Research Laboratory Industrial Associates, NIH grants DK 45533, HL 50855, and CA 74050, and US Army grant DAMD-17-94-J-4384.

Corresponding author e-mail: laura@essc.psu.edu.

  

muscle layer using a scalpel. In general, the distinction between those layers was quite well-defined. However, because the septum is thin, it was not divided but remained entirely with one of the layers. The "fat" section contained the skin and subcutaneous fat. The remainder of the specimen, bounded by the peritoneum, comprised the "muscle" section. This section consisted mainly of muscle but also included fatty intrusions, blood vessels, and tendons. Boundaries of both muscle and fat layers remained smooth after dissection. Markings corresponding to those on the skin were added on the top of the muscle layer. Distortion measurements were made for the individual layers using the same protocol as for the whole specimens, with the receiving aperture located as in the original measurement.

The measured wavefronts were characterized by computing the arrival time fluctuations, energy level fluctuations, and waveform similarity factor as in [6]. The arrival time and energy level variations determined for each data set were displayed as two-dimensional grayscale maps and their magnitudes were described in terms of rms values.

### *B. Simulations*

Propagation of ultrasonic pulses through the fat and muscle layers of the abdominal wall was simulated using the tissue modeling technique and finite-difference time-domain (FDTD) algorithm discussed in Ref. [5]. The six tissue maps of abdominal wall cross sections employed in the previous simulation study (not the specimens used in the measurements reported above) were used as input to the FDTD program, but in this case the tissue maps were divided into fat and muscle layers along the center of the septum between these layers, and the propagation of an ultrasonic pulse through each layer was calculated individually.

The tissue maps were made by processing scanned images of stained abdominal wall cross sections [7]. Regions containing connective tissue (e.g. skin, tendon, and septa), muscle, and fat were color coded. Density and sound speed arrays for the finite-difference computation were created from these images by mapping the various colors to representative density and sound speed values obtained from the literature for each tissue type. The values employed are reported in Ref. [5]. Representative sectional tissue maps are shown in Fig. 1.

In each case, the subcutaneous fat consists of lobules separated by thin connective tissue membranes (septa). Inhomogeneities, mainly consisting of fat, are present in all the muscle sections. This general appearance is consistent with descriptions from standard anatomical texts [8] and dissections of human specimens shown in Ref. [9]. The boundaries between muscle, fat, skin, and water (exterior to the specimen) in the maps of Fig. 1 are not entirely smooth or parallel. The roughness evident here is likely substantially greater than that occurring *in vivo* because the specimens were frozen before being sliced, and then fixed in formalin.

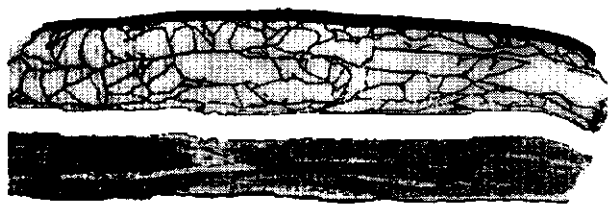

Fig. 1. Tissue maps for specimen 120fe. Black denotes connective tissue, dark gray denotes muscle, and light gray denotes fat. The fat layer (above) and the muscle layer (below) are obtained by dividing the map for the whole specimen (not shown).

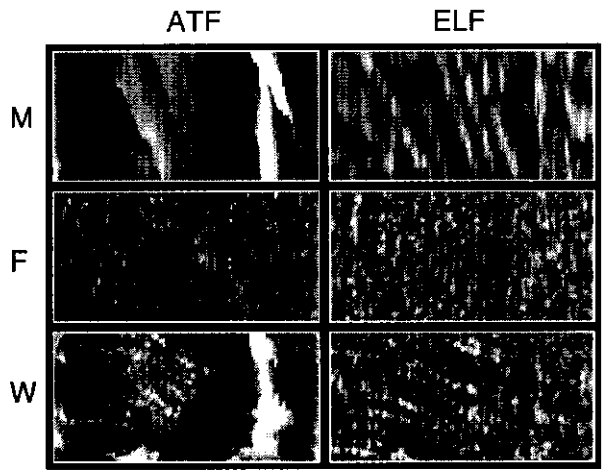


Fig. 2. Distortion maps for specimen 65. Energy level fluctuations (ELF) and arrival time fluctuations (ATF) are shown for the muscle layer (M), fat layer (F), and whole specimen (W). ATFs are shown on a linear gray scale with white indicating a delay of 150 ns and black indicatting an advance of 150 ns. ELFs are shown on a logarithmic gray scale with white indicating an increase of 10 dB and black indicating a decrease of 10 dB.

Simulated waveform data was processed using a one-dimensional version of the reference waveform method [5].

## III. Results

Measured arrival time and energy level fluctuation maps for representative muscle, fat, and whole abdominal wall sections are shown in Fig. 2. The distortion produced by the fat and muscle layers has distinctly different spatial characteristics. The muscle layers produce distortion patterns having strong anisotropy associated with the fibrous muscle structure. A white banded structure, corresponding to a large-scale delay in the wavefront, is seen at the position of a fatty aponeurosis that joins two muscle sections. The arrival time and energy level fluctuation maps for the fat layers, on the other hand, appear to consist almost entirely of small speckle-like structures. In the distortion maps for whole specimens, the striations and strong patterns of the muscle fluctuation maps are blended with the speckle created by the fat layer.

Statistics given in Table I summarize the measured distortion for all six specimens. These data indicate that the muscle layers measured caused significantly more severe

TABLE I. Distortion statistics (mean ± st. dev.) for the muscle layer (M), fat layer (F), and whole specimen (W) for measurements and FDTD simulations, each using six abdominal wall specimens.

| | | ATF (ns) | ELF (dB) | WSF |
|---|---|---|---|---|
| Meas. | M | 45.0 ± 17.8 | 2.79 ± 0.48 | 0.940 ± 0.023 |
| | F | 29.4 ± 11.5 | 2.96 ± 0.44 | 0.922 ± 0.061 |
| | W | 56.0 ± 16.4 | 3.15 ± 0.20 | 0.883 ± 0.048 |
| FDTD | M | 31.3 ± 18.1 | 1.70 ± 0.74 | 0.996 ± 0.005 |
| | F | 35.4 ± 11.2 | 3.50 ± 0.45 | 0.982 ± 0.010 |
| | W | 52.2 ± 14.1 | 3.62 ± 0.55 | 0.968 ± 0.017 |

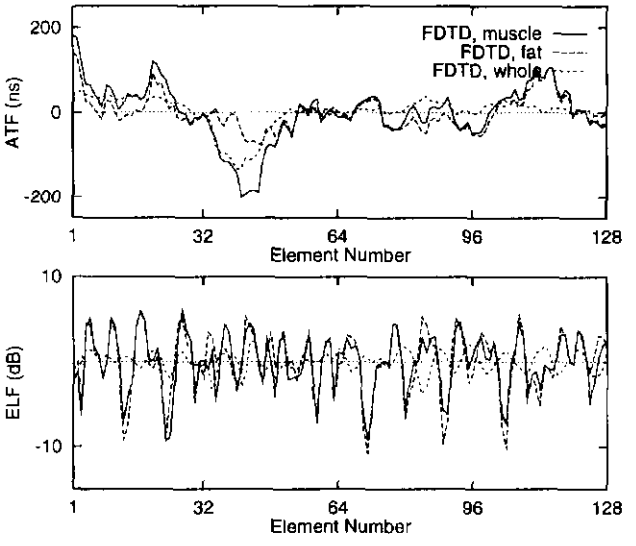


Fig. 3. Arrival time fluctuations (ATF) and energy level fluctuations (ELF) for specimen 120fe and its muscle and fat layers.

arrival time fluctuations than did the fat layers. The fat layers produced slightly more energy level distortion than the muscle layers and exhibit slightly more wave shape distortion as well. The arrival time, energy level, and wave shape distortion produced by whole specimens is generally greater than that produced by the individual layers, but is less than the arithmetic sum of the individual distortions combined.

Representative arrival time and energy level fluctuations simulated using whole abdominal wall specimens, muscle layers, and fat layers are shown in Fig. 3. The corresponding waveforms are shown in Fig. 4. In both these figures, large-scale arrival time fluctuations are seen that match well between muscle layers and whole specimens. Likewise, rapidly-varying energy level fluctuations seen for the fat layer are similar to those for the whole specimen. Furthermore, the waveforms are qualitatively similar to measured waveforms for abdominal wall specimens.

Statistics summarizing the distortion produced by the six tissue maps using the FDTD simulation are also presented in Table I. Overall, the muscle sections produced distortion of lower amplitude than did the corresponding fat layers. As with the measurements, the whole specimens usually produced more distortion than either of the layers but less

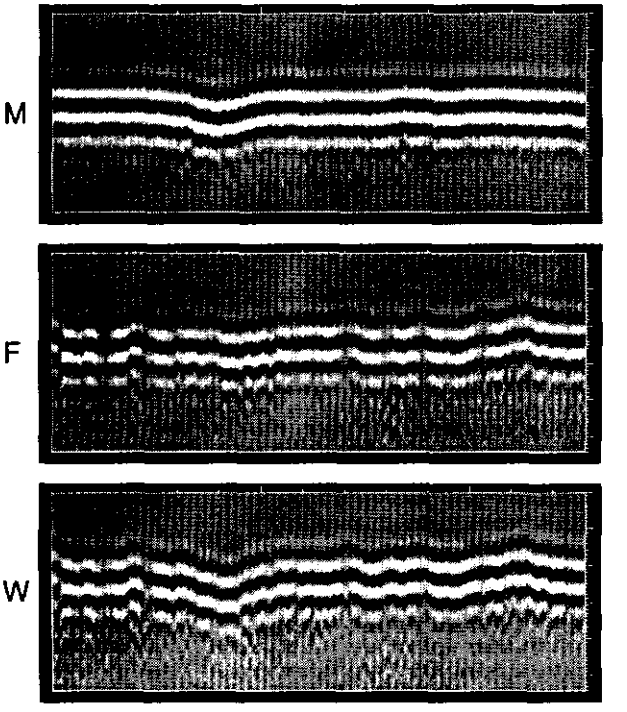


Fig. 4. Simulated waveforms for specimen 120fe (W) and its muscle (M) and fat (F) layers. Waveforms are shown on a linear gray scale with time as the vertical axis and element number as the horizontal axis. The temporal range shown is 2.3 $\mu$s for 128 elements.

than the total distortion of the two component specimens combined. Waveform similarity factors for simulations are generally higher than those for measured data using the same specimens.

Simulations of propagation through the abdominal wall provide additional insight into the relationships between specific tissue features and wavefront distortion characteristics. Two examples are shown in Figs. 5 and 6. Fig. 5 shows four successive frames of the ultrasonic pulse propagating through a muscle layer including a fatty aponeurosis, showing the development of a large-scale time-shift aberration. Fig. 6 shows four frames of the same pulse propagating through subcutaneous fat and septa after passing through the muscle layer. Here, scattering from thin septa causes energy to be scattered outside the main direction of propagation, resulting in significant amplitude dropouts. The processes by which distortion is produced are more easily observed in animations of the simulated wavefront propagation. Animated visualizations similar to Figs. 5 and 6 can be accessed from the web site http://www.personal.psu.edu/tdm104.

## IV. Discussion

Measurements and simulations of distortion made using human abdominal wall specimens and their individual fat and muscle layers have shown that both fat and muscle cause significant wavefront and focus distortion. The spatial characteristics of the resulting distortion are directly

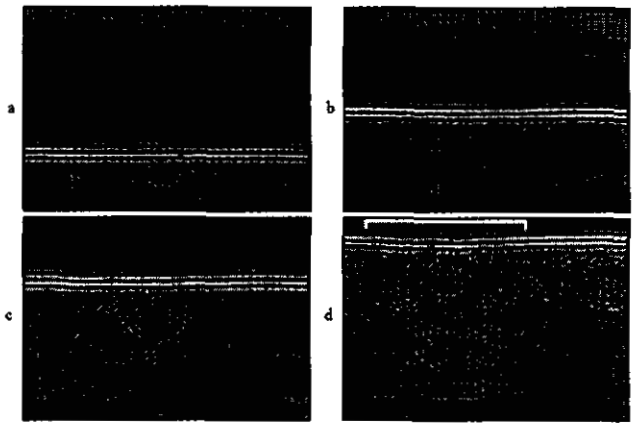


Fig. 5. Propagation through an aponeurosis in cross section 120fe. The area shown in each frame is 16.0 mm in height and 18.7 mm in width, while the temporal interval between frames is 1.7 $\mu$s. The tissue is represented by dark gray for connective tissue, medium gray for muscle, and light gray for fat. The wavefronts are shown on a bipolar logarithmic scale with a 30 dB dynamic range with white representing maximum positive pressure and black representing maximum negative pressure. A cumulative delay of about 0.2 $\mu$s, associated with propagation through the aponeurosis, is indicated by the square bracket in panel (d).

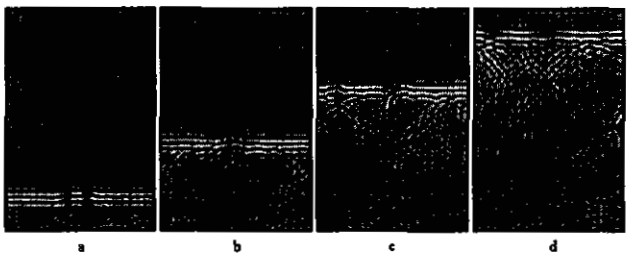


Fig. 6. Propagation through fat and septa in cross section 120fe. Panels *a)–d) show the progression of the main wavefront through* subcutaneous fat, showing amplitude dropouts caused by scattering from septa. The area shown in each frame is 22.9 mm in height and 14.4 mm in width, while the interval between frames is 3.8 $\mu$s. The tissue and wavefronts are represented as in Fig. 3.

related to the differences in internal tissue structure. The results imply that distortion caused by ultrasonic propagation through the abdominal wall is due to a more complex combination of effects than previously supposed by many researchers and clinicians.

On the whole, measurements show that muscle layers cause greater arrival time distortion but less energy level and waveform distortion. The ordered, fibrous structure of muscle causes greater anisotropy in observed distortion patterns. Smaller arrival time distortion in simulated propagation through muscle layers is probably due to inaccurate representation of fibrous microstructure.

Fat layers were found to cause less arrival time distortion but greater energy level and waveform distortion than muscle layers. These results, as well as the random anisotropic appearance of distortion patterns measured for fat sections, imply that scattering from septa is the primary cause of wavefront distortion in the subcutaneous fat. This conclusion is supported by the high energy level fluctuations seen in simulated propagation through fat layers.

Distortion caused by entire abdominal wall specimens has been shown experimentally to be a combination, but not a simple summation, of distortion effects caused by muscle and fat layers. Since most features from the muscle and fat distortion maps are clearly evident in the whole-specimen distortion maps, it may be concluded that internal tissue structures are more significant to ultrasonic wavefront distortion than any effects due to the muscle-fat boundary.

Simulation results support conclusions arrived at from the measurements. Specifically, the finite-difference simulation results show that both fat and muscle layers cause significant distortion. Comparable arrival time fluctuation is caused by muscle and fat layers. Energy level fluctuation caused by fat layers is greater in magnitude and more highly correlated with tissue structure than that produced by muscle layers.

Visualization of propagation through tissue, as seen in Figs. 5 and 6 and the corresponding animated sequences, has provided specific insight into the causes of ultrasonic wavefront distortion in transabdominal imaging. Large inhomogeneities, such as the aponeurosis of Fig. 5, cause significant arrival-time distortion on length scales comparable to the inhomogeneity size. Smaller features, such as septa within the subcutaneous fat, cause strong scattering effects that produce both waveform distortion and amplitude fluctuations.

## REFERENCES

[1] Y. Sumino and R. C. Waag, "Measurements of ultrasonic pulse arrival time differences produced by abdominal wall specimens," J. Acoust. Soc. Am. **90**(6), *2924–2930 (1991).*

[2] L. M. Hinkelman, D.-L. Liu, L. A. Metlay, and R. C. Waag, "Measurements of ultrasonic pulse arrival time and energy level variations produced by propagation through abdominal wall," J. Acoust. Soc. Am. **95**(1), 530–541 (1994).

[3] L. Ødegaard, E. Halvorsen, B. Ystad, H. G. Torp, and B. Angelsen, "Delay and amplitude focusing through the body wall; A simulation study," 1996 IEEE Ultrason. Symp. Proc. **2**, 1411–1414 (1996).

[4] A. P. Berkhoff, P. M. van den Berg, and J. M. Thijssen, "Simulation of wave propagation through aberrating layers of biological media," 1994 IEEE Ultrason. Symp. Proc. **3**, 1797–1800 (1994).

[5] T. D. Mast, L. M. Hinkelman, M. J. Orr, V. W. Sparrow, and R. C. Waag, "Simulation of ultrasonic pulse propagation through the abdominal wall," J. Acoust. Soc. Am. **102**(2), 1177–1190 (1997).

[6] L. M. Hinkelman, D.-L. Liu, R. C. Waag, Q. Zhu, and B. D. Steinberg, "Measurement and correction of ultrasonic pulse distortion produced by the human breast," J. Acoust. Soc. Am. **97**(3), 1958–1969 (1995).

[7] L. M. Hinkelman, L. A. Metlay, C. J. Churukian, and R. C. Waag, "Modified Gomori trichrome stain for macroscopic tissue slices," J. Histotech. **19**(4), 321–323 (1996).

[8] R. Warwick and P. L. Williams, Eds. *Gray's Anatomy*, 35th Ed. (W. B. Saunders, Philadelphia, 1973), pp. 40–41, 488–493, 519–527.

[9] L. M. Hinkelman, T. D. Mast, L. A. Metlay, and R. C. Waag, "The effect of abdominal wall morphology on ultrasonic pulse distortion. Part I. Measurements," submitted to J. Acoust. Soc. Am. (1997).